Three-Dimensional Imaging of Opaque Nanostructures in Silicon Chips Based on Ultrafast Optoacoustic Scanning Microscopy

JIE HUANG, YI HE, GUOJIE LUO and ZHONGQING SU

ABSTRACT

The recent advances in micromanufacturing have been pushing boundaries of the new generation of semiconductor devices, which, in the meantime, brings new challenges in material and structural characterization. An ultrafast laser-enable optoacoustic characterization methodology is developed in this work, targeting *in situ* calibration and delineation of the three-dimensional (3-D), nanoscopic interior features of opaque semiconductor chips. With the guidance of ultrafast electron-phonon coupling effect and velocity-perturbated optical interference, a femtosecond-laser pump-probe set-up based on Sagnac interferometer is configured to generate and acquire picosecond ultrasonic bulk waves (P-UBWs) traversing the microchips. The interior features of the microchips shift the phase of acquired P-UBW signals, reflected in the perturbed probe laser beam. The phase shifts are calibrated to compute signal correlation of P-UBW signals between different acquiring positions, whereby delineating the interior features in an intuitive manner. The approach is experimentally validated by characterizing nanoscopic, invisible interior aurum (Au)-gratings with periodically varied depths in typical microchips. Results highlight that the 3-D nanoscopic features of the microchips can be revealed with a microscopic and a nanoscopic spatial resolution, respectively along the transverse and depth directions of the chip, where the Au-gratings become "visible" with a depth variance of a few tens of nanometers only. This proposed approach has provided a fast, nondestructive approach to "see" through an opaque microchip with a nanoscopic resolution.

Department of Mechanical Engineering, The Hong Kong Polytechnic University, Kowloon, Hong Kong SAR

INTRODUCTION

Micromanufacturing has advanced the interior architectures of semiconductor devices with densified transistors, enhanced system integrity and remarkably boosted computational performance [1] yet without a necessary to reduce the transistor size or increase of the device volume. While 3-D microchip manufacturing offers significant advantages, its complex architecture creates major challenges for *in situ* nanoscale metrology [2,3]. Key obstacles include inaccessible internal features due to material opacity, potential sample damage from contact-based methods, and limitations in real-time implementation. These factors complicate non-destructive inspection of embedded structures and fine details. Furthermore, manufacturing defects like debonding, voids, and cracks [4,5] necessitate metrological approaches that can provide high-resolution, 3-D assessments of the interior features.

Various metrologies, including super-resolution optical microscopy [6] , scanning electron microscopy (SEM) [7], atomic force microscopy (AFM) [8], and X-ray tomography [9], have been developed to characterize micro- to nanoscale features in semiconductor chips. However, applying these methods to 3-D microchips involves trade-offs between precision, invasiveness, and *in situ* feasibility. Optical microscopy is non-invasive but lacks nanoscale resolution and material penetration. SEM offers nanoscale imaging but requires vacuum conditions, hindering *in situ* use. AFM achieves sub-nanometer surface resolution. However, it cannot probe buried structures.

Given these constraints, ultrafast optoacoustic metrology, employs ultrashort laser pulses with a duration of tens to hundreds of femtoseconds to generate ultrasonic waves from gigahertz (GHz) to terahertz (THz) has emerged as a transformative approach [10-15], eliminating the need for couplants and offering non-destructive, nanometer-scale resolution, volumetric imaging capabilities that circumvent the limitations of conventional techniques for nanoscale internal analysis of semiconductor devices.

In this work, a specialized ultrafast optoacoustic approach is developed. A femtosecond-laser pump-probe set-up configured with a Sagnac interferometer is established, which can identify the geometry of opaque nanoscopic interior features sandwiched inside 3-D micromanufacturing microchips. In the configured set-up, a milliwatt visible femtosecond-laser beam is responsible for the generation of P-UBWs, referred as to the pump beam. And the polarization of a microwatt infrared fs-laser beam, being the probe beam, is modulated to be sensible to the particulate velocity of P-UBWs in the Sagnac interferometer. Measurement is conducted for the nanoscopic aurum- (Au-) grating sandwiched between a silica-substrate and aluminum- (Al-) encapsulation, which mocks the senior of 3-D micromanufacturing microchips. The P-UBW signals are acquired, optimized, and processed for “see” through the geometry of opaque Au-grating.

EXPERIMETAL VALIDATION

Our experiments are performed using a femtosecond laser-based pump-probe system, which is illustrated in Fig. 1. The 1030 nm femtosecond laser source generates 50 fs pulses at a repetition rate of 807 kHz with an averaged power of 10 W. Then the output laser beam is directed into two directions by a 9:1 nonpolarized beam splitter. The stronger beam passes through an acousto-optic modulator (AOM) which modulates

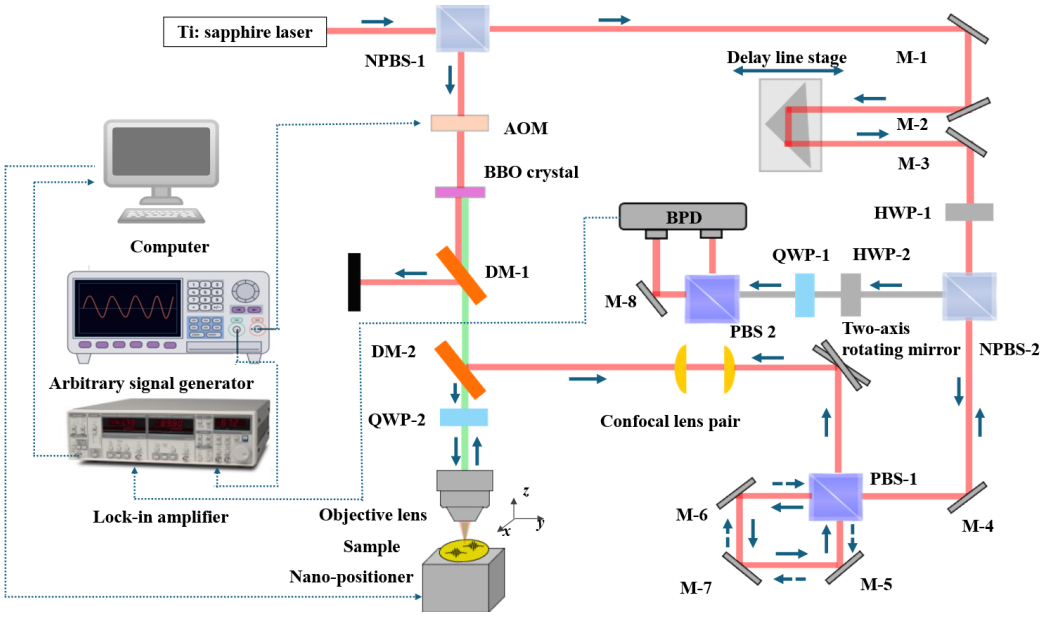

Figure 1. The schematic of the configurated femtosecond-laser pump-probe set-up.

the beams at 10 kHz and is subsequently frequency-doubled in a beta barium borate crystal (BBO) to generate 515 nm pump pulses. The other 1030 nm beam used as probe is firstly guided into the mechanical delay stage (ODL), with varied delay time by changing the optical path length between the pump and probe. Then, the probe beam is guided into a Sagnac interferometer with a motorized *yz*-motion stage. The Sagnac interferometer contains two half-wavelength plates (HWP-1 and -2), two quarter-wavelength plates (QWP-1 and -2), two polarized beam splitters (PBS-1 and -2), a nonpolarized beam splitter (NPBS-2), two convex lenses, and a balanced photodetector (BPD). The probe beams adjusted by the Sagnac interferometer possess particulate-velocity-sensitive polarization and therefore are capable of measuring P-UBWs. The two beams are recombined on a dichroic mirror in a collinear geometry and then focused onto the same spot on the sample surface by a 100-fold-magnification objective lens (OL). The pump beam has a spot size of 0.7 μm diameter and an averaged power decreased to 2 mW, the probe beam is 1.4 μm in diameter and 50 μW in power. The measured signals are sent to a lock-in amplifier (LIA), which is synchronized with the AOM with a 10 kHz signal to extract extremely low amplitude signals containing information of interior nanostructures under the heavy ambient noise. The delay stage moves in a continuous, relatively slow fashion, and care is taken to limit scanning the delay too quickly to avoid smearing out of fast features in the measurements due to the 30 ms integration time of the LIA.

The sample illustrated in Fig. 2 is fabricated by using the lithography and e-beam deposition system. Firstly, the 100 nm an Au-layer with a thickness of 100 nm is deposited on the surface of silica substrate, which is 200 μm thick. Then, the grating patterns, with a period of 10 μm, are lithographically transferred for the mask to the Au layer, the peak and valley are both 5 μm and the height of the gratings is 40 μm. Finally, the Al deposition is plated on top of the Au gratings with the thickness of 2 μm.

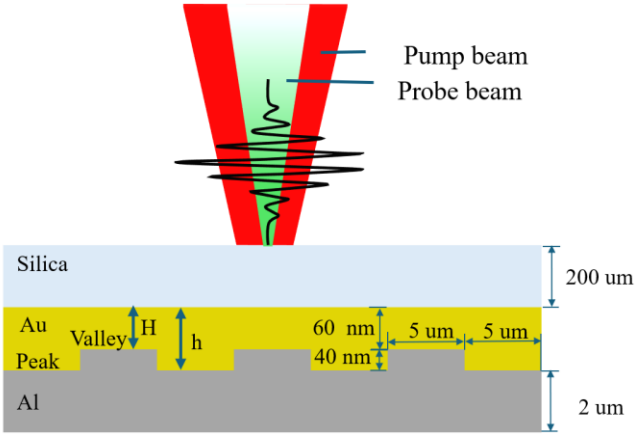

Figure 2. The cross-section view of the sample.

RESULTS

The P-UBW signals (Figs. 3a-b) exhibit collective oscillation due to superposition from multiple reflections in the subwavelength Au-grating, rather than discrete pulses. The oscillation frequency exceeds the central frequency, achieving ~20 dB signal-to-noise ratio (SNR) without averaging. While Au-grating thickness affects amplitude (stronger at valleys due to shorter travel distance) and phase, amplitude-based reconstruction is unreliable due to sensitivity to system factors, such as the reflectance of probe beams, surface roughness of objects, and the overall precision of alignment.

As illustrated in Fig. 3(d), comparative analysis of P-UBW signals acquired from the peak and valley regions of the Au-grating reveals a distinct phase-shifting phenomenon. This temporal shift arises from the propagation time difference of reflected P-UBWs, quantified as $2(H-h)/\upsilon_L$, where H and h denote the grating depths (Fig. 2) and υ_L represents the longitudinal wave phase velocity. The observed phase shift in the superimposed ultrasonic oscillations demonstrates remarkable robustness for Au-grating profilometry, being solely dependent on υ_L and thickness variation. Signal correlation analysis is employed to exploit this phase-shifting effect for dimensional characterization. Crucially, the invariant waveform of P-UBWs during correlation processing (Fig. 4) enables accurate measurement of grating features exceeding the ultrasonic wavelength. The correlation maxima occur at zero-time delay for valley-to-valley comparisons (Fig. 4a), indicating perfect phase matching. For peak-to-valley comparisons (Fig. 4b), 0.024 ns delay matches the theoretical $2(H-h)/\upsilon_L$ prediction. These measured delays are successfully applied to reconstruct the Au-grating profile (Fig. 4c), experimentally validating the nanoscale thickness resolution of this optoacoustic methodology.

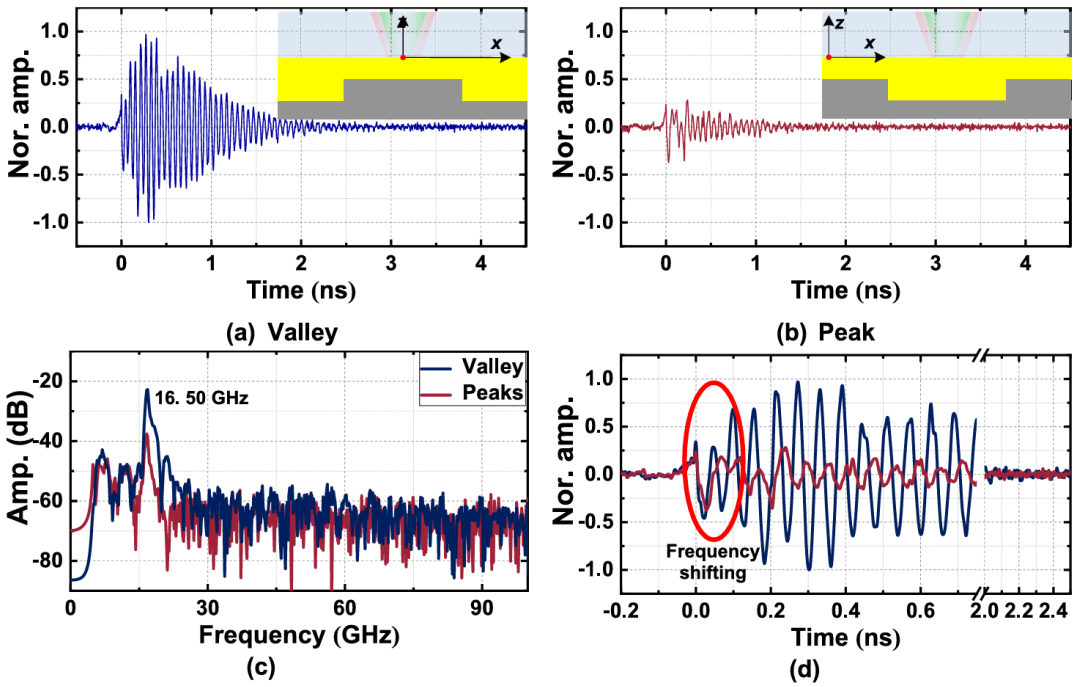

Figure 3. Measured P-UBW signals at (a) the valley and (b) the peak of the Au-grating, (c) the frequency spectrum corresponding to signals displayed in (a) and (b). (d) comparison between P-UBW signals showing a phase-shifting caused by the thickness difference between the peak and valley of Au-thickness, where the red ellipse frames out the signal segment with frequency shifting at initial periods.

DISCUSSION

While temporal scanning of P-UBWs remains fundamental to this methodology, significant improvements in measurement efficiency can be achieved through two complementary approaches. First, temporal optimization can be realized by selectively acquiring only the initial 1 ns interval of the P-UBW signals (Figs. 4a, b), which contains the highest amplitude responses following pump beam excitation. This targeted sampling strategy reduces the required measurement duration by 75% while maintaining sufficient signal integrity for correlation analysis. Second, a frequency-domain alternative employing Brillouin scattering spectroscopy offers the potential to circumvent spatial scanning entirely. This optical technique directly probes the spectral characteristics of P-UBWs, enabling the establishment of quantitative relationships between frequency-domain signatures and subsurface structural parameters, particularly layer thicknesses.

CONCLUSION

In conclusion, to address the challenges and gaps in *in situ* nanoscopic metrology for 3-D micromanufacturing microchips, an ultrafast optoacoustic approach is developed in this study. A femtosecond-laser pump-probe set-up, incorporating a Sagnac interferometer, is meticulously established to simultaneously generate and detect P-UBWs with contactless implementation.

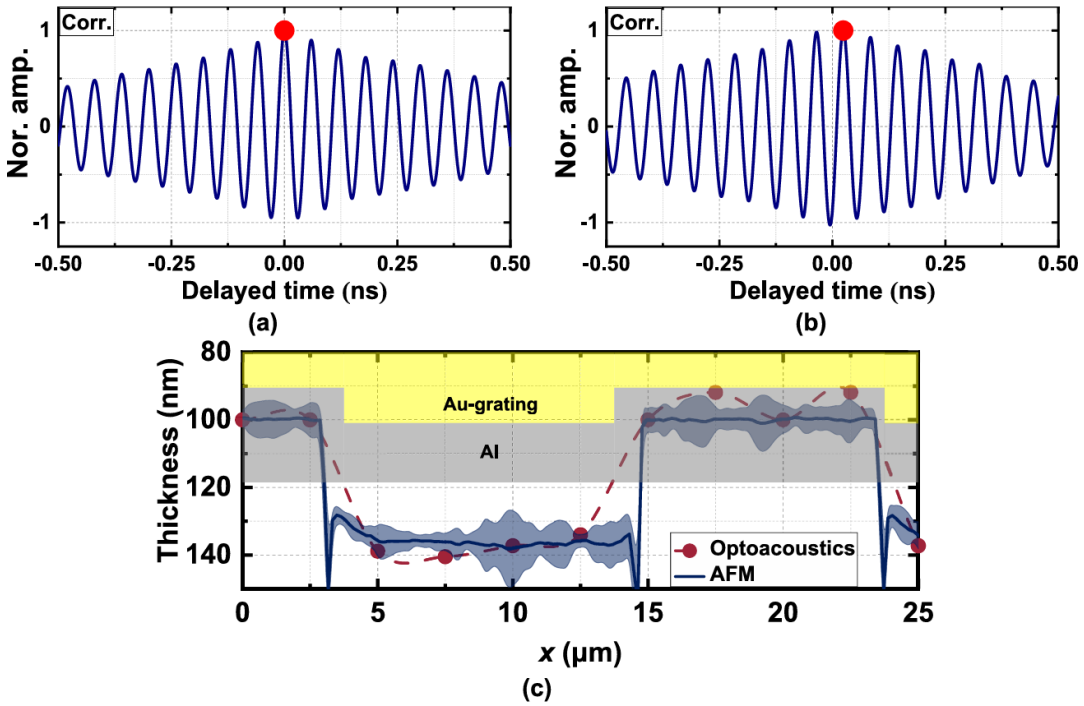

Figure 4. The correlation between two P-UBW signals sampled at (a) two peaks and (b) a peak and a valley of Au-grating, respectively, where the red spot signs the maximum correlation values. (c) the outlined profiles of Au-grating based on the correlation of phase-shifted signals measured using the proposed optoacoustic method and AFM, where the blue area represents the error bar of the AFM-based profile.

The technique exploits phase shifts in P-UBW signals induced by depth variations in embedded nanostructures (demonstrated using Au gratings between silica substrates and Al encapsulation layers), enabling inverse determination of subsurface features through signal correlation analysis. The optimized interferometric configuration achieves a remarkable 20 dB SNR without requiring signal averaging. Experimental results confirm that depth-dependent travel time differences of P-UBWs produce measurable phase shifts. Correlating P-UBWs signals across measurement positions, permitting accurate reconstruction of hidden nanostructures with nanoscale resolution. This robust and precise approach demonstrates the potential for meeting the critical needs of *in situ* metrology in advanced 3D semiconductor manufacturing.

REFERENCES

1. Sukumaran, V., Kumar, G., Ramachandran, K., Suzuki, Y., Demir, K., Sato, Y., Tummala, R. R. 2014. “Design, fabrication, and characterization of ultrathin 3-D glass interposers with through-package-vias at same pitch as TSVs in silicon,” *IEEE Trans. Compon., Packag., Manuf. Technol.*, 4(5):786-795.
2. Aryan, P., Sampath, S., & Sohn, H. 2018. “An overview of non-destructive testing methods for integrated circuit packaging inspection, ” *Sensors*, 18(7):1981.
3. Kwon, S., Park, J., Kim, K., Cho, Y., & Lee, M. 2022. “Microsphere-assisted, nanospot, non-destructive metrology for semiconductor devices,” *Light:Sci. Appl*, 11(1):32.
4. Chrostowski, L., Wang, X., Flueckiger, J., Wu, Y., Wang, Y., & Fard, S. T. 2014. “Impact of

fabrication non-uniformity on chip-scale silicon photonic integrated circuits," Optical Fiber Communication Conference, San Francisco, USA.
5. Koneru, A., Kannan, S., & Chakrabarty, K. 2017. "Impact of electrostatic coupling and wafer-bonding defects on delay testing of monolithic 3-D integrated circuits," *ACM J. Emerg. Technol. Comput. Syst.*, 13(4):1-23.
6. Nguyen, D. T., Mun, S., Park, H., Jeong, U., Kim, G.-h., Lee, S., Kim, D. 2022. "Super-resolution fluorescence imaging for semiconductor nanoscale metrology and inspection," *Nano Lett.*, 22(24):10080-10087.
7. Nakamae, K. 2021. "Electron microscopy in semiconductor inspection," *Meas. Sci. Technol.*, 32(5):052003.
8. Mathew, P. T., Rodriguez, B. J., & Fang, F. 2020. "Atomic and close-to-atomic scale manufacturing: a review on atomic layer removal methods using atomic force microscopy," *Nanomanuf. Metrol.*, 3(3):167-186.
9. Schmidt, C. 2018. "3-D X-Ray imaging with nanometer resolution for advanced semiconductor packaging: A review," *IEEE Trans. Compon., Packag., Manuf. Technol.*, 8(5):745-749.
10. Gusev, V. E., & Karabutov, A. 1991. "Laser optoacoustics," *NASA STI/Recon Tech. Rep. A*, 93: 16842.
11. Wright, O. B. 1994. "Ultrafast nonequilibrium stress generation in gold and silver," *Phys. Rev. B*, 49(14):9985.
12. Wright, O. B., & Gusev, V. 1996. "Ultrafast acoustic phonon generation in gold," *Phys. B Condens. Matter*, 219:770-772.
13. Matsuda, O., Larciprete, M. C., Voti, R. L., & Wright, O. B. 2015. "Fundamentals of picosecond laser ultrasonics," *Ultrasonics*, 56:3-20.
14. He, Y., Sohn, H., Matsuda, O., & Su, Z. 2023. "Optical polarization perturbed by shear strains of ultrasonic bulk waves in anisotropic semiconductors: Multiphysics modeling and optoacoustic validation," *Photoacoust.*, 32:100540.
15. Tomoda, M., Kubota, A., Matsuda, O., Sugawara, Y., & Wright, O. B. 2023. "Time-domain Brillouin imaging of sound velocity and refractive index using automated angle scanning," *Photoacoust.*, 31:100486.